Metal–Organic Frameworks

DOI: 10.1002/anie.201406501

Chemical and Structural Stability of Zirconium-based Metal–Organic Frameworks with Large Three-Dimensional Pores by Linker Engineering**

*Suresh B. Kalidindi, Sanjit Nayak, Michael E. Briggs, Susanna Jansat, Alexandros P. Katsoulidis, Gary J. Miller, John E. Warren, Dmytro Antypov, Furio Corà, Ben Slater, Mark R. Prestly, Carlos Martí-Gastaldo, and Matthew J. Rosseinsky**

Abstract: *The synthesis of metal–organic frameworks with large three-dimensional channels that are permanently porous and chemically stable offers new opportunities in areas such as catalysis and separation. Two linkers (L1 = 4,4′,4″,4‴-([1,1′-biphenyl]-3,3′,5,5′-tetrayltetrakis(ethyne-2,1-diyl)) tetrabenzoic acid, L2 = 4,4′,4″,4‴-(pyrene-1,3,6,8-tetrayltetrakis(ethyne-2,1-diyl))tetrabenzoic acid) were used that have equivalent connectivity and dimensions but quite distinct torsional flexibility. With these, a solid solution material, $[Zr_6O_4(OH)_4(L1)_{2.6}(L2)_{0.4}]\cdot(solvent)_x$, was formed that has three-dimensional crystalline permanent porosity with a surface area of over 4000 $m^2 g^{-1}$ that persists after immersion in water. These properties are not accessible for the isostructural phases made from the separate single linkers.*

Metal–organic frameworks (MOFs) are porous crystalline solids formed by the linking of organic and inorganic units.[1] Their chemically controllable crystalline porosity offers many scientifically interesting and technologically important advantages in areas, such as gas storage and separation,[2] heterogeneous catalysis,[3] sensing,[4] toxic gas removal,[5] drug delivery,[6] and proton conduction,[7] in bulk and thin films.[8] Although MOFs offer sizeable and chemically functionalizable three-dimensional porosity, which is very appealing for catalytic applications,[9] their performance is still limited by the need for materials with structural and hydrolytic stability along with high surface areas. To date, chemically stable architectures have been produced using nitrogen-based ligands[10] or by the combination of highly charged metal ions with carboxylates.[11–13] For example, the UiO-66,67,68 family,[12] based on octahedral Zr_6 oxo/hydroxo secondary building units (SBU), first demonstrated the ability of this Zr-SBU to produce water stable architectures with high surface areas (SA). However, their chemical stability (generally assessed by PXRD data) is reduced for UiO-67 and 68 as the pore volume increases.[14] We demonstrate how large (experimental BET surface area of 4184 $m^2 g^{-1}$), chemically stable three-dimensional pores can be produced by exploiting the synergy between two linkers of equivalent connectivity but distinct flexibility and chemistry: these properties are not accessible by one of the linkers in isolation. Stability is demonstrated by a range of techniques on analytically pure materials.

We prepared two tetrabenzoate linkers with the same four-fold connectivity and essentially identical metrics (Supporting Information, Table S8): 4,4′,4″,4‴-([1,1′-biphenyl]-3,3′,5,5′-tetrayltetrakis(ethyne-2,1-diyl)) tetrabenzoic acid

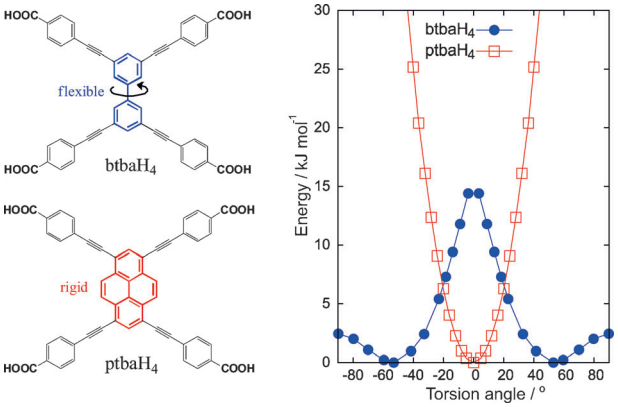

Scheme 1. The chemical structures of $btbaH_4$ and $ptbaH_4$ (left) are identical except for their core. As demonstrated by constrained molecular dynamics simulation data (right), a free $btbaH_4$ molecule has two symmetric non-planar equilibrium conformations in which the planes of the phenyl rings are rotated either clockwise or anticlockwise by 53° with respect to each other. In contrast, a free $ptbaH_4$ molecule with a rigid pyrene core has only one preferred conformation that is planar.

[*] Dr. S. B. Kalidindi,[+] Dr. S. Nayak,[+] Dr. M. E. Briggs, Dr. S. Jansat, Dr. A. P. Katsoulidis, Dr. G. J. Miller, Dr. J. E. Warren, Dr. D. Antypov, Dr. M. R. Prestly, Dr. C. Martí-Gastaldo, Prof. M. J. Rosseinsky
Department of Chemistry, University of Liverpool
Crown Street, Liverpool, L697ZD (UK)
E-mail: m.j.rosseinsky@liverpool.ac.uk
Dr. F. Corà, Dr. B. Slater
Department of Chemistry, University College London
WC1H 0AJ (UK)

[+] These authors contributed equally to this work.

[**] Financial support from EPSRC under EP/H000925, access to the HPC service ARCHER via EP/L000202. S.N. thanks the EU for a Marie Curie fellowship (PIEF-GA-2010-274952). C.M.-G. thanks the Spanish MINECO for a Ramón y Cajal Fellowship (RYC-2012-10894). We thank George Miller, Chemistry department, University of Liverpool for his assistance with ICP analysis.

Supporting information for this article is available on the WWW under http://dx.doi.org/10.1002/anie.201406501.

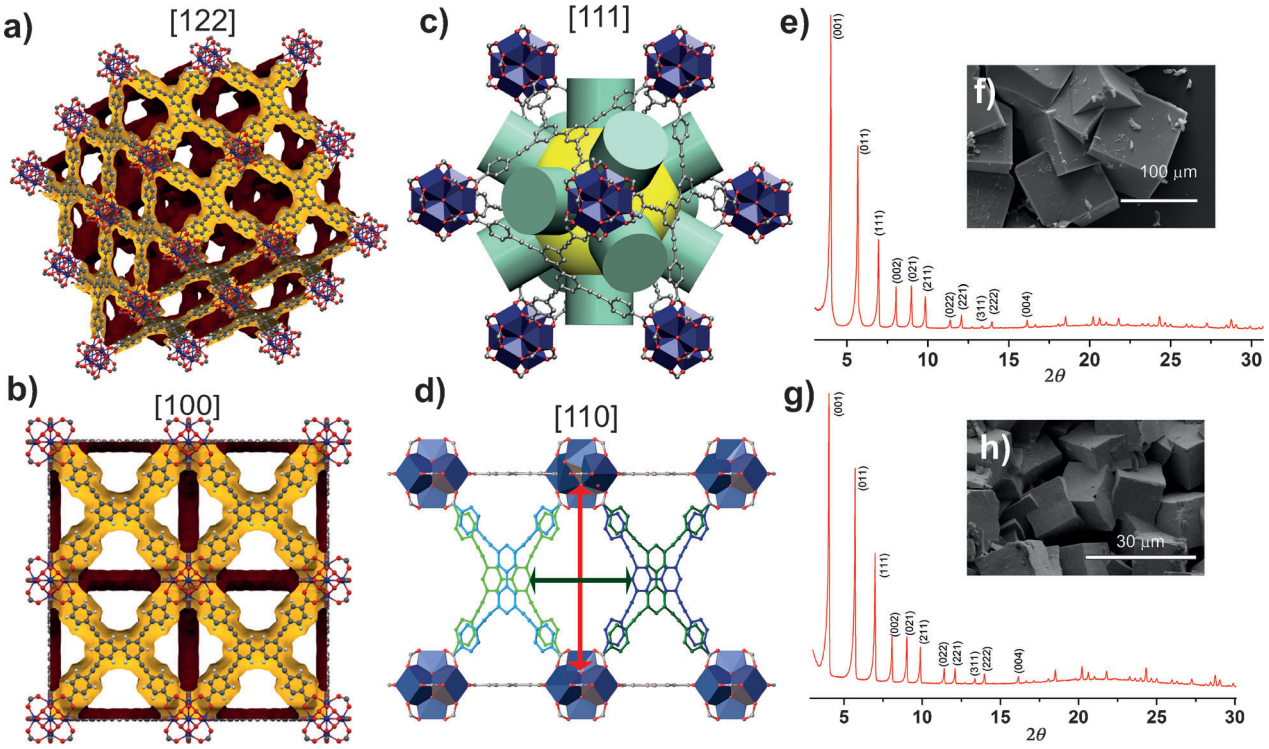

Figure 1. Structure and phase purity of as-made single linker phases. Single-crystal structure showing a 2×2×2 unit cell of **1** viewed along the [$\bar{1}2\bar{2}$] direction (a) and [100] direction (b); the three-dimensional porosity of **1** is shown by Connolly surfaces calculated using a 1.2 Å probe radius with the surfaces internal to the framework shown in yellow and the external surfaces shown in brown.[23] c) Cubic cages in **1** with an effective pore diameter of 18.7 Å indicated by the yellow sphere with maximum window diameters for a spherical probe of 7.6 Å indicated by the green cylinders. d) Four-membered windows interconnecting cubic cages along [110], the two crystallographically independent linker conformations are shown in dark blue and dark green with the symmetry equivalent linkers shown in light blue and light green, respectively. Maximal window dimensions based on measured minimum interatomic distances are 17.115(8) Å between the SBUs (direction indicated by the red arrow) and 12.783(4) Å between the linkers in parallel orientations (light blue–dark green), 11.815(4) Å between those in alternating orientations (light blue–dark blue) or 9.272(3) Å between those with a common orientation (light green–dark blue) (direction indicated by the dark green arrow). e) PXRD pattern of as-made **1**. f) SEM micrograph of as-made **1**. g) PXRD pattern of as-made **2**. h) SEM micrograph of as-made **2**.

($btbaH_4$) and 4,4′,4″,4‴-(pyrene-1,3,6,8-tetrayltetrakis-(ethyne-2,1-diyl))tetrabenzoic acid($ptbaH_4$) (Scheme 1). These linkers have quite different flexibility, which is due to the distinct nature of their cores. The pyrene-based $ptbaH_4$ linker is rigidly planar, whereas the biphenyl-based $btbaH_4$ linker has one extra torsional degree of freedom: there is a much lower barrier to torsion of the two sections of $btbaH_4$ (Supporting Information, Figure S35), which are twisted by 53° in the lowest energy conformer, and all of the torsional states are accessible within a 15 kJ mol^{-1} energy range corresponding to only a 30° torsion of $ptbaH_4$.

Reaction of anhydrous $ZrCl_4$ with $btbaH_4$ in DMF at 120 °C for three days in the presence of an excess of benzoic acid[15] yields cube-shaped light-green-colored single crystals of Zrbtba (**1**). Rotating-anode single-crystal X-ray diffraction shows **1** has the formula $[Zr_6O_4(OH)_4(btba)_3](DMF)_x(H_2O)_y$ and is metrically cubic in space group $Pm\bar{3}m$ (Supporting Information, Section S10a). Compound **1** is built from the $Zr_6O_4(OH)_4(CO_2)_{12}$ secondary building units (SBUs) characteristic of the UiO family,[12] with eight-coordinate Zr^{IV} atoms surrounded by 4 μ_3-O^{2-} or μ_3-OH^- and 4 μ_2-CO_2^- occupying the upper and lower faces of a square antiprism. The 4 μ_3-OH^- groups are arranged on opposing square faces to minimize electrostatic repulsion and yield an apolar SBU. The SBUs are interconnected by 12 tetracarboxylate btba linkers, one per edge of the octahedron, that in turn link four neighboring clusters to define a (12,4)-connected 3D framework with an **ftw** topology (Figure 1a,b).[16] The observed positional disorder of the linkers is best modelled in $R\bar{3}$, with a metrically cubic unit cell. Whereas combinations of these SBUs with linear dicarboxylate linkers generally produce (12,2)-connected 3D nets with face-centered cubic packing and **fcu**-type topologies, as exemplified by the UiO,[12] PIZOF,[17] PCN-56, to −59 families[13a] DUT-52,[18] or GU-MOMF-3,[19] the introduction of a tetradentate carboxylate such as btba results in an **ftw** connectivity as described for tetracarboxyphenylporphyrin struts in MOF-525 and similar systems.[20,21] Compound **1** displays a three-dimensional pore system formed by cubic micrometric cages with average pore diameters of 18.7 ± 0.1 Å (Figure 1c) connected by four-membered windows that can accommodate a spherical probe with a diameter of 7.6 Å along <110> (Figure 1d),[22] with a total calculated solvent-accessible volume of 8664.3 Å^3 (80.6% of the unit cell volume) (Supporting Information, Section S10).[24] Two btba linker orientations related by a two-fold rotation axis are visible from the crystallographic data

(Supporting Information, Figure S33(ii)) and there is pronounced elongation of the displacement ellipsoids along the normal to the ligand plane (Supporting Information, Figure S33(i)) that is indicative of significant deviations from planarity in the ligand conformation, consistent with the presence of both low-energy conformations in Scheme 1 (Supporting Information, Section S12).

These reaction conditions afford a material that is phase-pure (Figure 1e) by indexing and Pawley refinement (Supporting Information, Figure S40) of PXRD data, with the crystalline purity demonstrated by the homogeneous cubic habit of the crystallites in scanning electron microscopy (SEM) images (Figure 1f). The ^{1}H NMR spectrum (after digestion of MOF; Supporting Information, Figure S8) and TGA analysis (Supporting Information, Figure S14) of **1** showed the presence of a small (benzoic acid/linker = 0.18:3) amount of benzoic acid. The material has a composition of $[Zr_6O_4(OH)_4(C_{48}H_{22}O_8)_3](C_7H_6O_2)_{0.18}(H_2O)_5$ as demonstrated by CHN analysis (Supporting Information, Section S1d) and the agreement between predicted (25.4%) and observed (24.8%) ZrO_2 content in TGA experiments (Supporting Information, Figure S14), which remove the organic species in air.

Under the same reaction conditions, the $ptbaH_4$ ligand, which is less soluble in DMF, yielded a mixture of a crystalline Zrptba MOF **2** and an additional amorphous phase. Even though the amorphous phase remained undetected by PXRD, its presence is clearly evident from SEM data (Supporting Information, Figure S4) and unsatisfactory CHN analyses. $ptbaH_4$ is more soluble in NMP (*N*-methyl-2-pyrrolidone) than DMF, so we optimized the DMF/NMP ratio (Supporting Information, Figures S5, S6) to access phase pure **2** in 37.5% v/v NMP in DMF (Figure 1g) as orange red cubic crystals (Supporting Information, Figure S3), demonstrated by PXRD indexing (which gives similar metrics to **1**) and Pawley refinement and SEM images (Figure 1h). Single-crystal diffraction analysis shows that **2** (calculated void volume of 8386.0 Å^3, 78.9% of the cell volume) is effectively isostructural with **1**, with equivalent disorder of the tetradentate linkers. The average Zr–O/OH bond lengths in **1** and **2**, respectively 2.133(2) Å and 2.131(4) Å, are identical within experimental error, whereas the average distance between Zr and the carboxylate oxygen atoms are 2.231(2) Å in **1** and 2.216(3) Å in **2.**

In contrast to **1**, the CHN (Supporting Information, Section S1e) and TGA analytical data (Supporting Information, Figure S15) for phase-pure **2** do not agree well with the expected Zr/ligand ratio of two. Instead, the residual ZrO_2 content of 26.5 wt% (vs. 24.2 wt% expected for a stoichiometric material) is consistent with about 8% of the ptba linkers being missing and replaced with a hydroxide anion. This level of organic defect (one out of the twelve ligands bound to each SBU missing) is consistent with previous observations for UiO-66,[25] UiO-67,[25c] and PCN-225.[25d] The analytical data demonstrate the composition $[Zr_6O_4(OH)_4(C_{52}H_{22}O_8)_{2.75}(OH)](C_7H_6O_2)_{0.25}(H_2O)_2$ for **2**.[26] The observed (C 60.46, H 2.28) and predicted (C 60.09, H 2.47) CHN values are in very good agreement with the linker-deficient composition. Compound **2** is readily activated by heating under vacuum to remove the DMF and water guests to afford a three-dimensional porous material with a surface area of 4116 m^2g^{-1} and pore volume of 1.55 cm^3g^{-1} (Figure 2c,d).

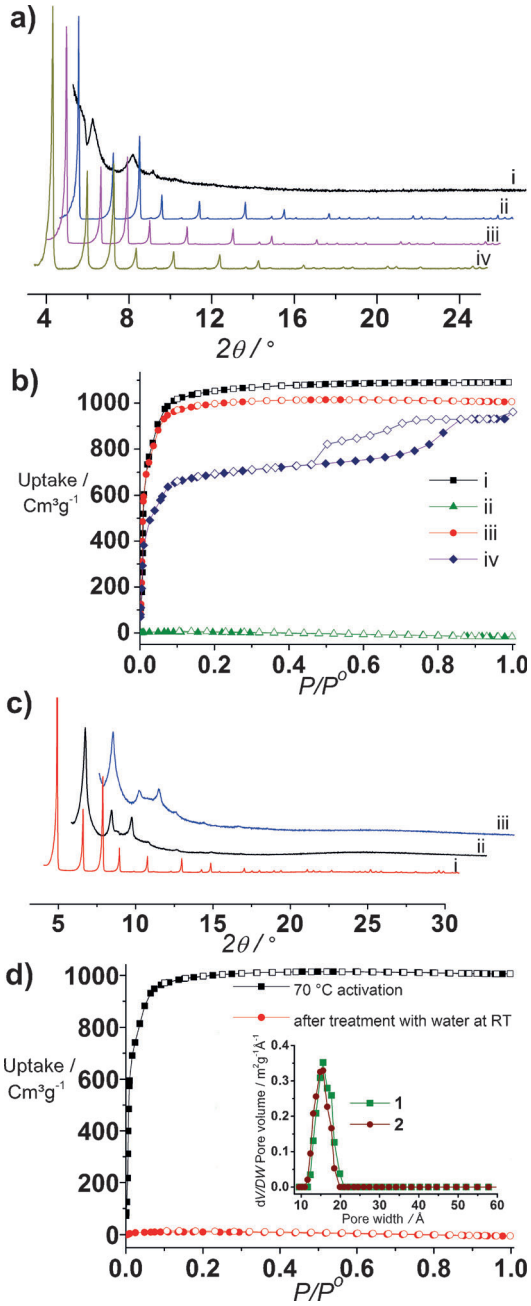

Figure 2. Evaluation of the chemical and structural stability of activated single linker phases by PXRD and N_2 isotherm measurement. a) PXRD patterns of **1** after i) activation at 70 °C, ii) activation with SCO_2, iii) treatment with water at RT followed by activation with SCO_2, and iv) treatment with water at 120 °C followed by activation with SCO_2. b) N_2 isotherms of **1** at 77 K after i) activation with SCO_2, ii) activation at 70 °C, iii) treatment with water at RT followed by activation with SCO_2, and iv) treatment with water at 120 °C followed by activation with SCO_2. c) PXRD patterns of **2** after i) activation at 70 °C; ii) treatment with water at RT followed by activation with SCO_2, and iii) treatment with water at 120 °C followed by activation with SCO_2. d) N_2 isotherms of **2** at 77 K after different treatments; the inset shows the DFT pore size distribution curves of **1** and **2**.

This BET surface area matches that computed based on the crystal structure, consistent with the analytical purity demonstrated above. The structurally robust permanent porosity can be ascribed to the rigidity of the ptba linker, despite the defect content observed, as in contrast significant care is required in activating btba-based **1** to attain the anticipated porosity. While simple thermal/vacuum activation (Supporting Information, Figure S19) results in collapse of the porosity (surface area of 0.3 $m^2 g^{-1}$), assigned to irreversible pore collapse by conformational change of the flexible linker, more careful activation of **1** by supercritical CO_2 (SCO_2) affords a surface area of 4342 $m^2 g^{-1}$ and pore volume of 1.68 $cm^3 g^{-1}$ (Figure 2a, b).[27] The pore size distribution curves (Figure 2d, inset) match the expected pore size of 18 Å from single-crystal data from **1** and **2**.

We assessed the chemical stability of flexible stoichiometric **1** and rigid defective **2** to water using the commonly applied visual inspection of PXRD patterns, but supplemented by ICP analysis of the supernatant solution and BET surface area and pore volume determination on the recovered solids after water treatment. Compound **1** is still crystalline (Figure 2a) after 48 h at room temperature (RT) and 120 °C water treatment, and does not leach to any extent even at 120 °C (0.00 wt % Zr at RT and 0.04×10^{-3} wt % at 120 °C is present in solution after these tests). However, **1** loses 7 % and 35 % of the initial BET surface area respectively under these conditions (to 4016 $m^2 g^{-1}$ and 2790 $m^2 g^{-1}$), with reduction of the pore volume to 1.57 $cm^3 g^{-1}$ and 1.43 $cm^3 g^{-1}$ (Figure 2b). Compound **2**, despite its increased structural rigidity and ease of activation to afford permanent porosity, is less chemically stable to both leaching (1.77×10^{-3} wt % Zr at RT and 0.347 wt % at 120 °C), PXRD (where the reflections broaden significantly; Figure 2c), and surface area measurements (Figure 2d; Supporting Information, Table S11). The surface area and pore volume of **2** decreased to 45 $m^2 g^{-1}$ and 0.00 $cm^3 g^{-1}$ after treatment with water at RT. DFT calculations (Supporting Information, Section S12) suggest that Zr leaching is enhanced by the defects in **2**.

These investigations show that the $btbaH_4$ ligand, based on the flexible biphenyl core, affords a stoichiometric MOF **1** with reasonable water stability, but which is not structurally stable to any but the most gentle activation of the porosity by guest removal. This lack of mechanical stability is attributed to the ease with which the flexible linker can deviate from planarity (Scheme 1) and block the pores. The rigid pyrene core of $ptbaH_4$ confers structural stability on guest-free **2**, but this linker-deficient structure is unstable in water: one four-connected linker cannot afford both types of robustness, but the integration of structural and chemical stability in a three-dimensional large pore high surface area framework is highly desirable.

The use of multiple linkers within a metal–organic framework has been shown to be a valuable route to tune structure and properties,[28] with behavior that is not a linear combination of that of the end-members being accessible.[29] As the synthetic conditions for **1** and **2** differ despite the similar connectivities of the linkers, control of the solvent affords a series of materials with increasing fractions of the rigid ptba linker. The starting molar ratios of $ptbaH_4$/$btbaH_4$ of 0.05, 0.47, and 1.69 afforded the molar linker ratios in the final materials of 0.15 **3A** (pure DMF), 1 **3B** (6.25 % v/v NMP in DMF), and 5.1 **3C** (12.5 % v/v NMP in DMF).

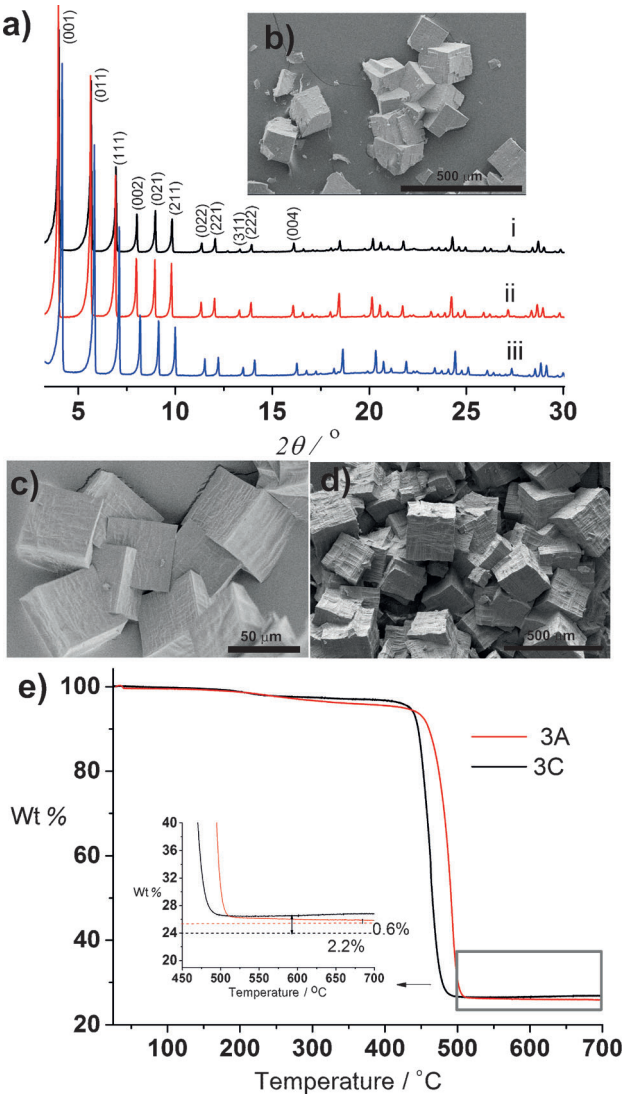

Figure 3. Structure and phase purity of mixed linker phases. a) PXRD patterns of as-made i) **3A**, ii) **3B**, iii) **3C**. b)–d) SEM images of as-made **3A**, **3B**, and **3C**, respectively. e) TGA profiles of **3A** and **3C** on heating in air. Inset: the final ZrO_2 mass expected for the stoichiometric Zr/linker ratio of two, as shown by dotted lines (red: **3A**, black: **3C**). In contrast to **3A**, the difference of 2.2% between calculated and observed residual ZrO_2 confirms the presence of about 8% missing linker defects in **3C**, which is further confirmed by CHN data.

SEM and PXRD data from **3A**, **3B**, and **3C** indicate they are all phase-pure (Figure 3a–d) and isostructural to **1** and **2**, with unit cell parameters in the same range (Supporting Information, Table S9). Similar to **2**, the CHN, NMR, and TGA data (Figure 3e) of **3C**, which has the highest content of the rigid ptba linker, confirms the presence of missing linker defects in the composition $[Zr_6O_4(OH)_4(C_{52}H_{22}O_8)_{2.30}(C_{48}H_{22}O_8)_{0.45}(OH)](C_7H_6O_2)_{0.2}(H_2O)_3$. For the systems with lower ptba content (**3A** and **3B**), the CHN, NMR, and TGA data are consistent with the formation of stoichio-

metric materials ($[Zr_6O_4(OH)_4(C_{48}H_{22}O_8)_{2.6}(C_{52}H_{22}O_8)_{0.4}]$-$(C_7H_6O_2)_{0.25}(H_2O)_4$ **3A** and $[Zr_6O_4(OH)_4(C_{48}H_{22}O_8)_{1.5}$-$(C_{52}H_{22}O_8)_{1.5}](C_7H_6O_2)_{0.45}(H_2O)_5$ **3B**) with a Zr/linker ratio of 2.0. Linker defects are thus associated with high fractions of the rigid ptba linker in the resulting MOF.

3B and **3C**, with 50% and 80% of the rigid ptba linker respectively, were activated under same conditions as succeeded for pure ptba-based **2**, affording BET surface areas of 4293 m^2g^{-1} and 4165 m^2g^{-1}, respectively (Supporting Information, Figures S20, S21). We also measured superatmospheric pressure adsorption isotherms of CO_2, CH_4, and N_2 on **3C** at 293 K and 18.5 bar (Supporting Information, Figure S23). Compound **3C** exhibits gravimetric uptake of CO_2 1070 $mg\,g^{-1}$ or 545 cm^3g^{-1}, slightly lower than MOF-177 and MOF-205[30] which adsorb about 1100 $mg\,g^{-1}$ (25 °C) and are two of the best mid-pressure-range (15–25 bar) CO_2 adsorbers. The CH_4 uptake of **3C** is 147 cm^3g^{-1} lower than HKUST-1 (185 cm^3g^{-1}, 25 °C) and PCN-14 (179 cm^3g^{-1}, 25 °C).[31] Like **2**, compounds **3B** and **3C** are not stable to water at room temperature (Supporting Information, Figure S52, Table S11). DFT calculations (Supporting Information, Section S12) suggest that the linker defects in **2** and **3C** decrease their stability to water. The relatively high rigid ptba content in stoichiometric **3B** distorts the linker-Zr_6 cluster bonding (owing to the slight mismatch in linker metrics; Supporting Information, Table S8) and lowers resistance to water attack. In contrast, **3A** is stable to water because it is defect-free and the incorporation of the rigid ptba linker induces no bond distortions. The enhanced mechanical stability of **3A** over pure btba-based **1** is conferred by the more rigid ptba.

Unlike pure bptba-based **1**, **3A** is stable to activation at 70 °C under 10^{-7} mbar to give the expected BET surface area of 4120 m^2g^{-1} and pore volume of 1.62 cm^3g^{-1} (Figure 4b). Incorporation of 15% $ptbaH_4$ into **1** has thus increased the structural stability of the guest-free framework dramatically. Compound **3A** is chemically stable to water attack at RT and comparison of the measures used show it is also superior to **1** in this regard (Figure 4c). The ICP analysis showed no detectable Zr leaching (Supporting Information, Table S10), and PXRD (Figure 4a) confirms that the structure of the MOF remains intact after soaking in water at RT for 48 h. Compound **3A** retains all of its surface area and pore volume (measured as 4184 m^2g^{-1} and 1.61 cm^3g^{-1} after exposure to water at RT for 48 h), as shown in Figure 4b, overcoming the poor stability of **2** in equivalent conditions. The synergy between the flexible btba and rigid ptba linkers affords an analytically pure multiple linker-based **3A** MOF displaying a three-dimensional pore system with a BET surface area above 4000 m^2g^{-1} that is hydrolytically and structurally stable at room temperature. This combination of properties is not accessible to the isostructural single linker phases thereby underpinning the value of the multilinker approach to produce porous solids with enhanced properties arising from synergy between linker chemistries.

Received: June 23, 2014
Revised: August 29, 2014

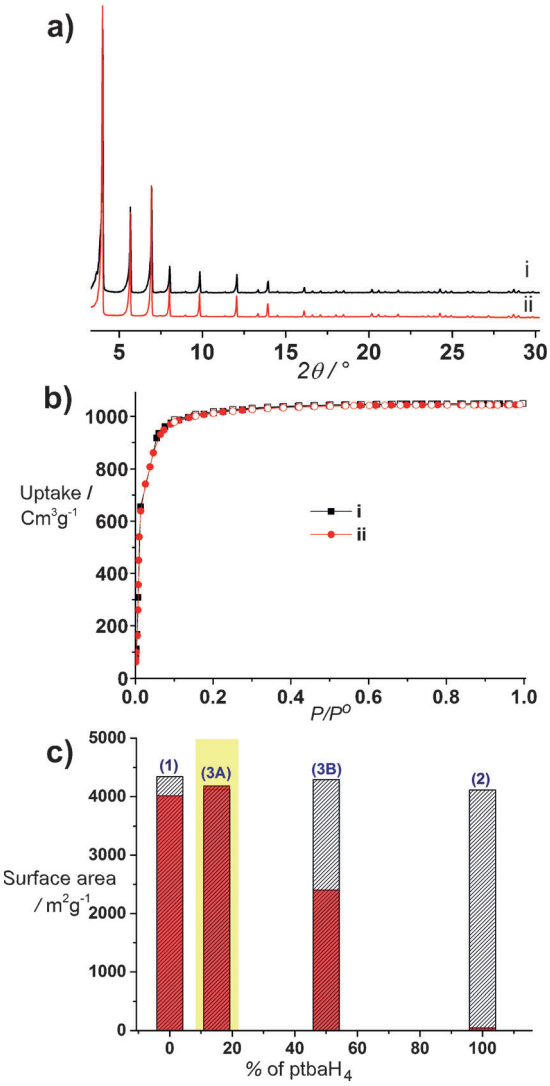

Figure 4. Combination of chemical and structural stability by the multiple linker approach. PXRD patterns (a) and N_2 isotherms (b) of **3A** i) after activation at 70 °C for which **1** collapses (Figure 2a, i) and ii) after treatment with water at RT followed by activation with SCO_2 for which **2** is not stable (Figure 2c, ii). c) Comparison of BET surface areas of **1**, **3A**, **3B**, and **2** before (white) and after (red) water treatment at room temperature. The yellow area highlights the optimum behavior of **3A**, which retains the same BET surface area after water treatment, unlike single linker **2** and multilinker **3B** with higher ptba content.

Keywords: mesoporous materials · metal–organic frameworks · water stability · zirconium

[1] a) H. Furukawa, K. E. Cordova, M. O'Keeffe, O. M. Yaghi, *Science* **2013**, *341*, 1230444; b) see the special issue on Metal–Organic Frameworks: *Chem. Rev.* **2012**, *112*, 673–1268; http://pubs.acs.org/toc/chreay/112/2; c) M. L. Foo, R. Matsuda, S. Kitagawa, *Chem. Mater.* **2014**, *26*, 310–322; d) G. Férey, C. Serre, *Chem. Soc. Rev.* **2009**, *38*, 1380–1399.

[2] a) J. R. Li, R. J. Kuppler, H. C. Zhou, *Chem. Soc. Rev.* **2009**, *38*, 1477–1504; b) B. V. Voorde, B. Bueken, J. Denayer, D. De Vos, *Chem. Soc. Rev.* **2014**, *43*, 5766–5788; c) E. D. Bloch, W. L. Queen, R. Krishna, J M. Zadrozny, C. M. Brown, J. R. Long,

Science **2012**, *335*, 1606 – 1610; d) Z. R. Herm, B. M. Wiers, J. A. Mason, J. M. Baten, M. R. Hudson, P. Zajdel, C. M. Brown, N. Masciocchi, R. Krishna, J. R. Long, *Science* **2013**, *340*, 960 – 964; e) H. Sato, W. Kosaka, R. Matsuda, A. Hori, Y. Hijikata, R. V. Belosludov, S. Sakaki, M. Takata, S. Kitagawa, *Science* **2014**, *343*, 167 – 170; f) J. R. Li, J. Sculley, H. C. Zhou, *Chem. Rev.* **2012**, *112*, 869 – 932.

[3] a) J. Y. Lee, O. K. Farha, J. Roberts, K. A. Scheidt, S. B. T. Nguyen, J. T. Hupp, *Chem. Soc. Rev.* **2009**, *38*, 1450 – 1459; b) M. Yoon, R. Srirambalaji, K. Kim, *Chem. Rev.* **2012**, *112*, 1196 – 1231; c) P. Garcìa-Garcìa, M. Müller, A. Corma, *Chem. Sci.* **2014**, *5*, 2979 – 3007; d) J. Liu, L. Chen, H. Cui, J. Zhang, L. Zhang, C. Su, *Chem. Soc. Rev.* **2014**, *43*, 6011.

[4] a) M. M. Wanderley, C. Wang, C.-D. Wu, W. Lin, *J. Am. Chem. Soc.* **2012**, *134*, 9050 – 9053; b) L. E. Kreno, K. Leong, O. K. Farha, M. Allendorf, R. P. Van Duyne, J. T. Hupp, *Chem. Rev.* **2012**, *112*, 1105 – 1125; c) V. Stavila, A. A. Talin, M. D. Allendorf, *Chem. Soc. Rev.* **2014**, *43*, 5994 – 6010.

[5] a) C. Montoro, F. Linares, E. Q. Procopio, I. Senkovska, S. Kaskel, S. Galli, N. Masciocchi, E. Barea, J. A. R. Navarro, *J. Am. Chem. Soc.* **2011**, *133*, 11888 – 11891; b) E. Barea, C. Montoro, J. A. R. Navarro, *Chem. Soc. Rev.* **2014**, *43*, 5419 – 5430.

[6] P. Horcajada, R. Gref, T. Baati, P. K. Allan, G. Maurin, P. Couvreur, G. Férey, R. E. Morris, C. Serre, *Chem. Rev.* **2012**, *112*, 1232 – 1268.

[7] a) M. Yoon, K. Suh, S. Natarajan, K. Kim, *Angew. Chem. Int. Ed.* **2013**, *52*, 2688 – 2700; *Angew. Chem.* **2013**, *125*, 2752 – 2764; b) S. Horike, D. Umeyama, S. Kitagawa, *Acc. Chem. Res.* **2013**, *46*, 2376 – 2384; c) P. Ramaswamy, N. E. Wong, G. K. H. Shimizu, *Chem. Soc. Rev.* **2014**, *43*, 5913 – 5932.

[8] A. Bétard, R. A. Fischer, *Chem. Rev.* **2012**, *112*, 1055 – 1083.

[9] M. J. Climent, A. Corma, S. Iborra, M. J. Sabater, *ACS Catal.* **2014**, *4*, 870 – 891.

[10] a) K. Park, Z. Ni, A. Côté, J. Choi, R. Huang, F. Uribe-Romo, H. Chae, M. O'Keeffe, O. M. Yaghi, *Proc. Natl. Acad. Sci. USA* **2006**, *103*, 10186 – 10191; b) A. Phan, C. J. Doonan, F. J. Uribe-Romo, C. B. Knobler, M. O'Keeffe, O. M. Yaghi, *Acc. Chem. Res.* **2010**, *43*, 58 – 67; c) V. Colombo, S. Galli, H. J. Choi, G. D. Han, A. Maspero, G. Palmisano, N. Masciocchi, J. R. Long, *Chem. Sci.* **2011**, *2*, 1311 – 1319.

[11] a) J. J. Low, A. I. Benin, P. Jakubczak, J. F. Abrahamian, S. A. Faheem, R. R. Willis, *J. Am. Chem. Soc.* **2009**, *131*, 15834 – 15842; b) H. Chevreau, T. Devic, F. Salles, G. Maurin, N. Stock, C. Serre, *Angew. Chem. Int. Ed.* **2013**, *52*, 5056 – 5060; *Angew. Chem.* **2013**, *125*, 5160 – 5164; c) G. Férey, C. Mellot-Draznieks, C. Serre, F. Millange, J. Dutour, S. Surblé, I. Margiolaki, *Science* **2005**, *309*, 2040 – 2042; d) C. Serre, F. Millange, C. Thouvenot, M. Noguès, G. Marsolier, D. Louër, G. Fére, *J. Am. Chem. Soc.* **2002**, *124*, 13519 – 13526.

[12] a) J. Cavka, S. Jakobsen, U. Olsbye, N. Guillou, C. Lamberti, S. Bordiga, K. Lillerud, *J. Am. Chem. Soc.* **2008**, *130*, 13850 – 13851; b) G. C. Shearer, S. Chavan, J. Ethiraj, J. G. Vitillo, S. Svelle, U. Olsbye, C. Lamberti, S. Bordiga, K. P. Lillerud, *Chem. Mater.* **2014**, *26*, 4068 – 4071.

[13] a) H. L. Jiang, D. Feng, T. F. Liu, J. R. Li, H. C. Zhou, *J. Am. Chem. Soc.* **2012**, *134*, 14690 – 14693; b) V. Guillerm, F. Ragon, M. Dan-Hardi, T. Devic, M. Vishnuvarthan, B. Campo, A. Vimont, G. Clet, Q. Yang, G. Maurin, G. Férey, A. Vittadini, S. Gross, C. Serre, *Angew. Chem. Int. Ed.* **2012**, *51*, 9267 – 9271; *Angew. Chem.* **2012**, *124*, 9401 – 9405.

[14] J. B. Decoste, G. W. Peterson, H. Jasuja, T. G. Glover, Y. G. Huang, K. S. Walton, *J. Mater. Chem. A* **2013**, *1*, 5642 – 5650.

[15] A. Schaate, P. Roy, A. Godt, J. Lippke, F. Waltz, M. Wiebcke, P. Behrens, *Chem. Eur. J.* **2011**, *17*, 6643 – 6651.

[16] O. Delgado-Friedrichs, M. O'Keeffe, O. M. Yaghi, *Phys. Chem. Chem. Phys.* **2007**, *9*, 1035 – 1043.

[17] A. Schaate, P. Roy, T. Preuße, S. J. Lohmeier, A. Godt, P. Behrens, *Chem. Eur. J.* **2011**, *17*, 9320 – 9325.

[18] V. Bon, I. Senkovska, M. S. Weiss, S. Kaskel, *CrystEngComm* **2013**, *15*, 9572 – 9577.

[19] S. A. K. Robinson, M.-V. L. Mempin, A. J. Cairns, K. T. Holman, *J. Am. Chem. Soc.* **2011**, *133*, 1634 – 1637.

[20] a) W. Morris, B. Volosskiy, S. Demir, F. Gándara, P. L. McGrier, H. Furukawa, D. Cascio, J. F. Stoddart, O. M. Yaghi, *Inorg. Chem.* **2012**, *51*, 6443 – 6445; b) D. Feng, H. Jiang, Y. Chen, Z. Gu, Z. Wei, H. Zhou, *Inorg. Chem.* **2013**, *52*, 12661 – 12667.

[21] a) Z. Chang, D. S. Zhang, T. L. Hu, X.-H. Bu, *Cryst. Growth Des.* **2011**, *11*, 2050 – 2053; b) X. Zhao, X. Wang, S. Wang, J. Dou, P. Cui, Z. Chen, D. Sun, X. Wang, D. Sun, *Cryst. Growth Des.* **2012**, *12*, 2736 – 2739; c) O. Delgado-Friedrichs, M. O'Keeffe, O. M. Yaghi, *Acta Crystallogr. Sect. A* **2006**, *62*, 350 – 355.

[22] T. F. Willems, C. H. Rycroft, M. Kazi, J. C. Meza, M. Haranczyk, *Microporous Mesoporous Mater.* **2012**, *149*, 134 – 141.

[23] Figure 1 a and b were generated using CCDC Mercury: C. F. Macrae, I. J. Bruno, J. A. Chisholm, P. R. Edgington, P. McCabe, E. Pidcock, L. Rodriguez-Monge, R. Taylor, J. van de Streek, P. A. Wood, *J. Appl. Crystallogr.* **2008**, *41*, 466 – 470.

[24] Total solvent-accessible void volumes were calculated using CALCSOLV implemented in Olex2: O. V. Dolomanov, L. J. Bourhis, R. J. Gildea, J. A. K. Howard, H. Puschmann, *J. Appl. Crystallogr.* **2009**, *42*, 339 – 341.

[25] a) H. Wu, Y. S. Chua, V. Krungleviciute, M. Tyagi, P. Chen, T. Yildirim, W. Zhou, *J. Am. Chem. Soc.* **2013**, *135*, 10525 – 10532; b) L. Valenzano, B. Civalleri, S. Chavan, S. Bordiga, M. H. Nilsen, S. Jakobsen, K. P. Lillerud, C. Lamberti, *Chem. Mater.* **2011**, *23*, 1700 – 1718; c) M. J. Katz, Z. J. Brown, Y. J. Colon, P. W. Siu, K. A. Scheidt, R. Q. Snurr, J. T. Hupp, O. K. Farha, *Chem. Commun.* **2013**, *49*, 9449 – 9451; d) H. L. Jiang, D. Feng, K. Wang, Z. Y. Gu, Z. Wei, Y. P. Chen, H. C. Zhou, D. Feng, Z. Y. Gu, J. R. Li, H. L. Jiang, Z. Wei, H. C. Zhou, *J. Am. Chem. Soc.* **2013**, *135*, 13934 – 13938.

[26] During the publication process of the present paper, Farha et al. reported a different protocol for the synthesis of a Zr-ptba MOF: O. V. Gutov, W. Bury, D. A. Gomez-Gualdron, V. Krungleviciute, D. F. -Jimenez, J. E. Mondloch, A. A. Sarjeant, S. S. Al-Juaid, R. Q. Snurr, J. T. Hupp, T. Yildirim, O. K. Farha, *Chem. Eur. J.* **2014**, *20*, 12389 – 12393.

[27] A. P. Nelson, O. K. Farha, K. L. Mulfort, J. T. Hupp, *J. Am. Chem. Soc.* **2009**, *131*, 458 – 460.

[28] a) H. Deng, C. J. Doonan, H. Furukawa, R. B. Ferreira, J. Towne, C. B. Knobler, B. Wang, O. M. Yaghi, *Science* **2010**, *327*, 846 – 850; b) T. Fukushima, S. Horike, Y. Inubushi, K. Nakagawa, Y. Kubota, M. Takata, S. Kitagawa, *Angew. Chem. Int. Ed.* **2010**, *49*, 4820 – 4824; *Angew. Chem.* **2010**, *122*, 4930 – 4934; c) A. D. Burrows, *CrystEngComm* **2011**, *13*, 3623 – 3642; d) S. Henke, A. Schneemann, A. Wütscher, R. A. Fischer, *J. Am. Chem. Soc.* **2012**, *134*, 9464 – 9474; e) T. Lescouet, E. Kockrick, G. Bergeret, M. Pera-Titus, S. Aguado, D. Farrusseng, *J. Mater. Chem.* **2012**, *22*, 10287 – 10293.

[29] C. Martí-Gastaldo, D. Antypov, J. E. Warren, M. E. Briggs, P. A. Chater, P. V. Wiper, G. J. Miller, Y. Z. Khimyak, G. R. Darling, N. G. Berry, M. J. Rosseinsky, *Nat. Chem.* **2014**, *6*, 343 – 351.

[30] H. Furukawa, N. Ko, Y. B. Go, N. Aratani, S. B. Choi, E. Choi, A. Ö. Yazaydin, R. Q. Snurr, M. O'Keeffe, J. Kim, O. M. Yaghi, S *cience* **2010**, *329*, 424 – 428.

[31] J. A. Mason, M. Veensra, J. R. Long, *Chem. Sci.* **2014**, *5*, 32 – 51.

